Ab initio calculation of the effective on-site Coulomb interaction parameters for half-metallic magnets

Ersoy Şaşıoğlu,[1,*] Iosif Galanakis,[2,†] Christoph Friedrich,[1] and Stefan Blügel[1]

[1]*Peter Grünberg Institut and Institute for Advanced Simulation, Forschungszentrum Jülich and JARA, D-52425 Jülich, Germany*
[2]*Department of Materials Science, School of Natural Sciences, University of Patras, GR-26504 Patra, Greece*

Correlation effects play an important role in the electronic structure of half-metallic (HM) magnets. In particular, they give rise to nonquasiparticle states above (or below) the Fermi energy at finite temperatures that reduce the spin polarization and, as a consequence, the efficiency of spintronics devices. Employing the constrained random-phase approximation (cRPA) within the full-potential linearized augmented-plane-wave (FLAPW) method using maximally localized Wannier functions, we calculate the strength of the effective on-site Coulomb interaction (Hubbard U and Hund exchange J) between localized electrons in different classes of HM magnets considering: (i) sp-electron ferromagnets in rock-salt structure, (ii) zinc-blende $3d$ binary ferromagnets, as well as (iii) ferromagnetic and ferrimagnetic semi- and full-Heusler compounds. For HM sp-electron ferromagnets, the calculated Hubbard U parameters are between 2.7 and 3.9 eV, while for transition-metal-based HM compounds, they lie between 1.7 and 3.8 eV, being smallest for MnAs (Mn-$3d$ orbitals) and largest for Cr_2CoGa (Co-$3d$ orbitals). For the HM full-Heusler compounds, the Hubbard U parameters are comparable to the ones in elementary $3d$ transition metals, while for semi-Heusler compounds, they are slightly smaller. We show that the increase of the Hubbard U with structural complexity, i.e., from MnAs to Cr_2CoGa, stems from the screening of the p electrons of the nonmagnetic sp atoms. The p-electron screening turns out to be more efficient for MnAs than for Cr_2CoGa. The calculated Hubbard U parameters for CrAs, NiMnSb, and Co_2MnSi are about two times smaller than previous estimates based on the constrained local-density approximation (cLDA) method. Furthermore, the width of the correlated d or p bands of the studied compounds is usually smaller than the calculated Hubbard U parameters. Thus these HM magnets should be classified as weakly correlated materials.

I. INTRODUCTION

The field of spintronics is one of the most rapidly expanding fields of nanoscience and technology because the incorporation of the electron's spin offers an additional degree of freedom to be used for information processing in nanodevices.[1] A key role in this research field is played by *ab initio* studies of the electronic structure within density functional theory (DFT), which have allowed the modeling of the properties of several materials prior to their experimental growth. Among the materials that might find application in future magnetic nanodevices are the half-metallic (HM) magnets.[2,3]

The ferromagnetic semi-Heusler compound NiMnSb was the first material for which the HM character was predicted and described;[4] it exhibits usual metallic behavior for one spin direction, while an energy gap in the band structure is present in the other spin direction as in semiconductors. The prospect of creating 100% spin-polarized current has triggered interest in such compounds and since the initial prediction of de Groot *et al.* several HM compounds have been discovered.[5,6] Several aspects concerning the implementation of HM alloys in realistic devices, like magnetic tunnel junctions, spin valves, and spin transistors, have been discussed in literature.[7–10]

For HM magnets, mean-field calculations of the electronic structure, such as DFT, yield 100% spin polarization at the Fermi level. However, correlation effects among the localized electrons lead to the appearance of nonquasiparticle states above (or below) the Fermi level at finite temperatures. These states stem from the electron-magnon interaction and

cannot be described within DFT irrespective of the correlation strength. The existence of these states has been experimentally confirmed by recent magnetic tunnel junction spectroscopy measurements on the ferromagnetic HM full-Heusler compound Co_2MnSi.[11] Nonquasiparticle states severely affect the perfect spin polarization above (or below) the Fermi level degrading the performance of spintronics devices. Moreover, their behavior is material specific and thus extensive calculations of the electronic structure of half-metals are needed including correlation effects.

Electronic structure calculations based on DFT with local or semilocal approximations for the exchange-correlation functional are quite successful for materials from weak to intermediate electronic correlations. However, they fail for systems with strong electronic correlations. There are two common ways to include correlations in first-principles electronic structure calculations. The first one is the so-called LDA+U scheme in which the local density approximation (LDA) of DFT is augmented by an on-site Coulomb repulsion term and an exchange term with the Hubbard U and Hund exchange J parameters, respectively.[12,13] Such a scheme has been applied, for example, to Co_2FeSi, showing that correlations restore the HM character of the compound,[14] and to NiMnSb.[15] However, LDA+U cannot describe the nonquasiparticle states. A more elaborate modern computational scheme, which combines many-body model Hamiltonian methods with DFT, is the so-called LDA + DMFT method, where DMFT stands for dynamical mean-field theory.[16,17] In this scheme, the interacting many-body system is mapped onto the subspace of

localized states, formed by d or p orbitals in the present compounds, where the interaction with the rest of the system is again incorporated in a Hubbard U and Hund exchange J parameter. The still very complex many-body problem in the correlated subspace is solved as an Anderson impurity problem embedded in a dynamical mean field—in the form of a frequency-dependent self-energy—that accounts for all other sites. LDA + DMFT has been applied to several HM magnetic systems like Co_2MnSi,[11] NiMnSb,[18–20] FeMnSb,[21] Mn_2VAl,[22] VAs,[23] and CrAs.[24,25] Indeed, in all these compounds the LDA + DMFT method yielded nonquasiparticle states above (or below) the Fermi energy.

Thus the Coulomb interaction parameters (Hubbard U and Hund exchange J) play a crucial role in the study of the correlation effects in solids. However, their determination from experimental data is a difficult task, which impedes the predictive power of these approaches. Therefore a direct calculation of these parameters in solids from first principles is highly desirable. Several authors have addressed this problem and a number of different approaches have been proposed and applied to the bulk phase of various classes of materials.[26–39] Among them, the constrained local-density approximation (cLDA) is the most popular,[29–31] but cLDA is known to give unreasonably large Hubbard U values for the late transition metal atoms due to difficulties in compensating for the self-screening error of the localized electrons.[33] On the other hand, the constrained random-phase approximation (cRPA), though numerically much more demanding, does not suffer from these difficulties and offers an efficient way to calculate the effective Coulomb interaction parameters in solids. Moreover, cRPA allows to determine individual Coulomb matrix elements, e.g., on site, off site, intraorbital, interorbital, and exchange, as well as their frequency dependence.[32,35]

Despite enormous work on HM magnets, no determination of the Coulomb interaction parameters exists within the cRPA approach. Available cLDA calculations of Hubbard U parameter for HM CrAs, NiMnSb, and Co_2MnSi turned out to be unreasonably large (6–7 eV). Thus previous studies employing the Hubbard U either assume values close to the ones of the elementary transition metal (TM) atoms or are performed for a variety of Hubbard U values.[14] On the other hand, previous cRPA calculations for TMs have shown that the Hubbard U values are sensitive to a variety of factors like the crystal structure, the spin polarization, the d electron number, and the d orbital filling,[35] and thus values for the elementary TMs cannot be directly used for complex intermetallic compounds. The aim of the present work is to present a systematic study of the effective on-site Coulomb interaction parameters (Hubbard U and Hund exchange J) between localized d or p electrons in 20 HM magnets. We consider representatives of the (i) semi-Heusler compounds like NiMnSb, (ii) ferrimagnetic full-Heusler compounds like Mn_2VAl, (iii) inverse full-Heusler compounds like Cr_2CoGa, (iv) usual $L2_1$-type ferromagnetic full-Heusler compounds, (v) transition-metal pnictides like CrAs, and finally (vi) sp-electron (also called d^0) ferromagnets like CaN. Thus our study covers a wide range of HM magnets allowing for a deeper understanding of the behavior of the Coulomb interactions parameters of the same element in different HM magnetic systems. To calculate the effective Coulomb interaction parameters, we

have employed the cRPA method within the full-potential linearized augmented-plane-wave (FLAPW) method using maximally localized Wannier functions (MLWFs).

The paper is organized as follows. In Sec. II, we shortly present the methodology behind cRPA calculations. In Sec. III, we present calculated values of Coulomb interaction parameters for a variety of well-known HM magnets. Finally, we summarize our conclusions in Sec. IV.

II. COMPUTATIONAL METHOD

All compounds considered in this paper crystallize in a cubic structure as shown in Fig. 1. The lattice consists of four interpenetrating fcc lattices with Wyckoff positions: A = (0 0 0), B = $(\frac{1}{4} \frac{1}{4} \frac{1}{4})$, C = $(\frac{1}{2} \frac{1}{2} \frac{1}{2})$, and D = $(\frac{3}{4} \frac{3}{4} \frac{3}{4})$. In the case of the rock-salt (RS) [zinc-blende (ZB)] structure, the B and D (C and D) sites are vacant. In the $C1_b$-type structure adapted by the semi-Heusler compounds (XYZ), the X,Y, and Z atoms occupy the A, B, and D sites, respectively, and the C site is vacant. Full-Heusler compounds possess either the $L2_1$-type or the XA-type structure depending on the valency of the X and Y elements. If the valency of the X elements is larger (smaller) than that of the Y element, the compound prefers the $L2_1$-(XA)-type structure. In the XA-type structure, the unit cell is occupied in the sequence X-X-Y-Z instead of the X-Y-X-Z sequence in the $L2_1$-type structure; the two X atoms are not anymore equivalent. For the HM Heusler compounds as well as for some zinc-blende systems, we have used experimental lattice parameters, while for the sp-electron ferromagnets theoretical ones are used (see Table I). The ground-state calculations are carried out using the FLAPW method as implemented in the FLEUR code[40] with the generalized gradient approximation (GGA) to the exchange-correlation potential as parameterized by Perdew *et al.*[41] A dense $16 \times 16 \times 16$ **k**-point grid is used to perform the numerical integrations in the Brillouin zone. The maximally localized Wannier functions (MLWFs) are constructed with the WANNIER90 code.[42–44] The effective Coulomb potential is calculated within the recently developed cRPA method[32–34] implemented in the SPEX code[45] (for further technical details see Refs. 35 and 46). We use an $8 \times 8 \times 8$ **k**-point grid in the cRPA calculations. In the rest of the section, we will sketch the formalism used to calculate the effective Coulomb potential.

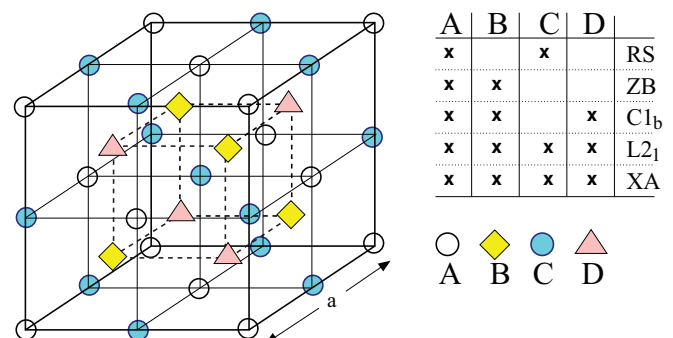| A	B	C	D	
x		x		RS
x	x			ZB
x	x		x	$C1_b$
x	x	x	x	$L2_1$
x	x	x	x	XA

FIG. 1. (Color online) Schematic representation of the cubic structure of the various lattices adopted by the present compounds. The cube contains exactly four primitive unit cells.

TABLE I. Crystal structures (RS stands for rock salt and ZB for zinc blende), lattice constants, atom-resolved, interstitial, and total spin magnetic moments (in μ_B) for all considered HM magnets. Lattice constants are taken from Refs. 61, 63, 71, 74, and 80.

Comp.	Str.	a(Å)	m_A	m_B	m_C	m_D	m_{Int}	m_T
CaN	RS	5.02	0.05		0.79		0.16	1.00
SrN	RS	5.37	0.04		0.81		0.15	1.00
SrC	RS	5.67	0.13		1.15		0.72	2.00
BaC	RS	6.00	0.14		1.15		0.71	2.00
VAs	ZB	5.69	1.89	−0.15			0.17	2.00
CrAs	ZB	5.65	2.99	−0.25			0.26	3.00
MnAs	ZB	5.65	3.58	−0.17			0.27	3.68
FeMnSb	C1$_b$	5.88	−1.14	3.13		−0.03	0.04	2.00
CoMnSb	C1$_b$	5.87	−0.21	3.29		−0.09	0.01	3.00
NiMnSb	C1$_b$	5.93	0.25	3.72		−0.06	0.09	4.00
Mn$_2$VAl	L2$_1$	5.93	−1.55	1.00	−1.55	0.03	0.07	−2.00
Mn$_2$VSi	L2$_1$	5.76	−0.73	0.43	−0.73	0.02	0.03	−0.98
Cr$_2$FeGe	XA	5.76	−1.23	1.51	−0.27	−0.01	0.03	0.03
Cr$_2$CoGa	XA	5.80	−1.94	1.72	0.42	−0.05	−0.08	0.07
Co$_2$CrAl	L2$_1$	5.73	0.80	1.55	0.80	−0.07	−0.08	3.00
Co$_2$CrSi	L2$_1$	5.65	1.00	2.04	1.00	−0.05	0.01	4.00
Co$_2$MnAl	L2$_1$	5.76	0.77	2.73	0.77	−0.10	−0.12	4.05
Co$_2$MnSi	L2$_1$	5.65	1.05	3.01	1.05	−0.06	−0.05	5.00
Co$_2$FeAl	L2$_1$	5.73	1.22	2.80	1.22	−0.07	−0.17	5.00
Co$_2$FeSi	L2$_1$	5.64	1.37	2.82	1.37	−0.01	−0.07	5.48

In the present work, the correlated d or p subspace is spanned by a set of MLWFs, which are given by

$$w_{n\mathbf{R}}^{\sigma}(\mathbf{r}) = \frac{1}{N} \sum_{\mathbf{k}} e^{-i\mathbf{k}\cdot\mathbf{R}} \sum_{m} T_{\mathbf{R},mn}^{\sigma}(\mathbf{k}) \varphi_{\mathbf{k}m}^{\sigma}(\mathbf{r}), \quad (1)$$

where N is the number of $\mathbf{k}$ points, $T_{\mathbf{R},mn}^{\sigma(\mathbf{k})}$ is the unitary transformation matrix, $\varphi_{\mathbf{k}m}^{\sigma}(\mathbf{r})$ are single-particle Kohn-Sham states of spin σ and band index m, and $\mathbf{R}$ is the atomic position vector in the unit cell. The transformation matrix $T_{mn}^{\sigma(\mathbf{k})}$ is determined by minimizing the spread

$$\Omega = \sum_{n,\sigma} \left(\langle w_{n\mathbf{0}}^{\sigma} | r^2 | w_{n\mathbf{0}}^{\sigma} \rangle - \langle w_{n\mathbf{0}}^{\sigma} | \mathbf{r} | w_{n\mathbf{0}}^{\alpha} \rangle^2 \right), \quad (2)$$

where the sum runs over all Wannier functions. We choose the p states as our correlated subspace for rocksalt sp-electron materials, while for zinc-blende and Heusler compounds the d states form the correlated subspace.

Within the RPA, the polarization function is written as

$$P(\mathbf{r},\mathbf{r}';\omega) = \sum_{\sigma} \sum_{\mathbf{k},m}^{occ} \sum_{\mathbf{k}',m'}^{unocc} \varphi_{\mathbf{k}m}^{\sigma}(\mathbf{r}) \varphi_{\mathbf{k}'m'}^{\sigma*}(\mathbf{r}) \varphi_{\mathbf{k}m}^{\sigma*}(\mathbf{r}') \varphi_{\mathbf{k}'m'}^{\sigma}(\mathbf{r}')$$
$$\times \left[\frac{1}{\omega - \Delta_{\mathbf{k}m,\mathbf{k}'m'}^{\sigma}} - \frac{1}{\omega + \Delta_{\mathbf{k}m,\mathbf{k}'m'}^{\sigma}} \right] \quad (3)$$

with $\Delta_{\mathbf{k}m,\mathbf{k}'m'}^{\sigma} = \epsilon_{\mathbf{k}'m'}^{\sigma} - \epsilon_{\mathbf{k}m}^{\sigma} - i\delta$, the Kohn-Sham eigenvalues $\epsilon_{\mathbf{k}m}^{\sigma}$, and a positive infinitesimal δ. The σ runs over both spin channels. The basic idea of the cRPA is to define an effective interaction U between the localized (correlated) electrons by restricting the screening processes to those that are not explicitly treated in the effective model Hamiltonian. To this end, we divide the full polarization matrix $P = P_l + P_r$, where

P_l includes transitions only between localized states and P_r is the remainder.

For the calculation of the polarization matrix P_l, we restrict the summation over the virtual transitions $m \to m'$ in Eq. (3) to those where both the initial and final states are elements of the correlated subspace. This is straightforward in materials where the subspace is formed by isolated bands so that the partitioning of states is unique. However, such a case is an exception. In most materials, as in most of those considered in the present work, the bands forming the subspace are entangled with other bands, and a clear separation is not possible. Here, we employ a method outlined in Ref. 35. We calculate for each state $\varphi_{\mathbf{k}m}^{\sigma}$ the probability $p_{\mathbf{k}m}^{\sigma}$ of finding an electron that resides in that state within the correlated subspace. From Eq. (1) it follows that $p_{\mathbf{k}m} = \sum_{\mathbf{R},n} |T_{\mathbf{R},mn}^{\sigma}(\mathbf{k})|^2$. The polarization matrix P_l is then calculated from Eq. (3) with the additional factor $p_{\mathbf{k}m}^{\sigma} p_{\mathbf{k}'m'}^{\sigma}$ for each term of the sum, i.e., for each virtual transition $\mathbf{k}m \to \mathbf{k}'m'$. For isolated bands, the factor $p_{\mathbf{k}m}^{\sigma} p_{\mathbf{k}'m'}^{\sigma}$ is simply either 0 or 1, the latter for virtual transitions that take place inside the correlated subspace, thus comprising the simple case where the partitioning of states is unique. Yet for the general case of entangled bands, one has $0 < p_{\mathbf{k}m}^{\sigma} p_{\mathbf{k}'m'}^{\sigma} < 1$.

With these definitions, the effective interaction is formally given by the matrix equation

$$U = [1 - vP_r]^{-1} v, \quad (4)$$

where v is the bare Coulomb matrix. It is related to the fully screened interaction $\tilde{U}$, where the screening from the localized electrons is also taken into account, by

$$\tilde{U} = [1 - vP]^{-1} v = [1 - UP_l]^{-1} U. \quad (5)$$

The U is nonlocal and inherits a frequency dependence from $P_r(\mathbf{r},\mathbf{r}';\omega)$. We consider matrix elements of U in the MLWF basis

$$U_{\mathbf{R}n_1n_3;n_4n_2}^{\sigma_1\sigma_2}(\omega) = \iint w_{n_1\mathbf{R}}^{\sigma_1*}(\mathbf{r}) w_{n_3\mathbf{R}}^{\sigma_1}(\mathbf{r}) U(\mathbf{r},\mathbf{r}';\omega)$$
$$\times w_{n_4\mathbf{R}}^{\sigma_2*}(\mathbf{r}') w_{n_2\mathbf{R}}^{\sigma_2}(\mathbf{r}') \, d^3r \, d^3r'. \quad (6)$$

The average Coulomb matrix elements U_{LDA+U}, U, U', and J are defined as follows:

$$U_{LDA+U} = \frac{1}{L^2} \sum_{m,n} U_{\mathbf{R}mn;mn}^{\sigma_1\sigma_2}(\omega=0), \quad (7)$$

$$U = \frac{1}{L} \sum_{m} U_{\mathbf{R}mm;mm}^{\sigma_1\sigma_2}(\omega=0), \quad (8)$$

$$U' = \frac{1}{L(L-1)} \sum_{m\neq n} U_{\mathbf{R}mn;mn}^{\sigma_1\sigma_2}(\omega=0), \quad (9)$$

$$J = \frac{1}{L(L-1)} \sum_{m\neq n} U_{\mathbf{R}mn;nm}^{\sigma_1\sigma_2}(\omega=0), \quad (10)$$

where L is the number of localized orbitals, i.e., three and five for p and d orbitals, respectively. We note that although the matrix elements of the Coulomb potential U are formally spin dependent due to the spin dependence of the MLWFs, we

find that this dependence is negligible in practice. [Henceforth, with U we refer to the average value, Eq. (8), rather than to the matrix, Eq. (4).]

Different conventions exist in the literature for the definition of the Hubbard U. (For a detailed discussion see Ref. 47.) Historically, the Hubbard U was introduced as a Coulomb repulsion parameter between electrons in the single-orbital Hubbard-Kanamori-Gutzwiller model.[48] Note that there is no Hund exchange J for a single orbital. For multiorbital systems, the Hubbard U is defined as the average intraorbital and interorbital Coulomb matrix elements. In the present work, we follow the convention used in Ref. 49 and denote the Hubbard U as U_{LDA+U} and the Hund exchange interaction as J [see Eqs. (7) and (10)]. As mentioned before, in contrast to cLDA, the cRPA approach allows to access individual Coulomb matrix elements and thus, in addition to U_{LDA+U}, we define the average intraorbital U and interorbital U' Coulomb interaction parameters in Eqs. (8) and (9), which are necessary for constructing the multiorbital model Hamiltonians. If the crystal field has a cubic symmetry, then the U' is given by $U' = U - 2J$. In this case, only two among U, U' and J are independent parameters. In multiorbital systems, the Hund exchange J favors spin polarization. Similarly to U, U', and J, we can also define the so-called fully screened $\tilde{U}$, $\tilde{U}'$, and $\tilde{J}$ [see Eq. (5)]. Although the fully screened Coulomb interaction matrix elements are not used in model Hamiltonians, they provide an idea about the correlation strength of the considered electrons.

Finally, we would like to note that different conventions of the Hubbard U parameter in the literature might be confusing for the reader aiming to use this parameter in LDA+U calculations. In usual LDA+U methods, the parameter U_{LDA+U} should be taken as the Slater integral F^0. It is also worth to note that there are two main LDA+U schemes which are in widespread use today. The Dudarev approach, in which an isotropic screened on-site Coulomb interaction $U_{eff} = U_{DFT+U} - J$, is used, and the Lichtenstein approach in which the U_{DFT+U} and exchange J parameters are treated separately.[50] The Dudarev approach is equivalent to the Lichtenstein approach for $J = 0$.[51] Both the effect of the choice of the LDA+U scheme on the orbital occupation and subsequent properties like the electronic band gap[52,53] as well as the dependence of the magnetic properties on the value of Hubbard U and Hund exchange J have been analyzed in the literature.[54–56] A better scheme for the LDA+U calculations would be to use the full Coulomb matrix with a proper treatment of the double counting issue.

III. RESULTS AND DISCUSSION

The results and discussion section is divided into four parts. In the first part, we present the results of self-consistent electronic structure calculations to establish the electronic and magnetic properties of the compounds under study. In the second part, we present the calculated Coulomb interaction parameters for all considered systems. The orbital and frequency dependence of the Coulomb interaction is discussed for selected compounds in the third and fourth part, respectively. The last part is devoted to the study of the role that the p

electrons of the nonmagnetic sp element play in the screening of the Coulomb interactions for three prototype systems.

A. Magnetic moments and half-metallicity

In the present study, we consider a variety of HM magnets, which are shown in Table I together with the structure, lattice constant, and the calculated spin magnetic moments in units of μ_B. The first family of compounds are the so-called sp-electron ferromagnets (also known as d^0 ferromagnets).[57,58] We consider the nitrides and the carbides (CaN, SrN, SrC, and BaC) since they have the largest calculated Curie temperatures among the studied sp-electron ferromagnets.[59–65] These compounds crystallize in the rocksalt structure and do not contain TM atoms. Electronic structure calculations show that they are magnetic, and their total spin magnetic moment in units of μ_B equals $8 - Z_t$, where Z_t is the total number of valence electrons in the unit cell. The latter are formally made up of the sp states of N or C, while the s state of the A element (Ca, Sr, or Ba) is located at such a low energy that it is not classified as a valence state. This rule for the total spin magnetic moment is known as Slater-Pauling (SP) behavior and was first identified in the transition-metal binary compounds.[66,67] The number 8 stems from the number of available sp states: four majority and four minority-spin states. The former (one of s character low in energy and three bonding p states) are all occupied, while the latter are only partially filled. So, $8 - Z_t$ is the number of unfilled minority-spin states and equals the total spin magnetic moment as a consequence. The Fermi level crosses the bonding minority-spin p states, and an energy gap forms in the majority states between the bonding and antibonding p states. As can be concluded from the spin-magnetic moment presented in Table I, all four compounds under study are half-metals with a total spin magnetic moment of 1 μ_B for the nitrides and 2 μ_B for the carbides. In the nitrides, the spin moment is carried mainly by the N atoms, while in the carbides a large portion of the spin magnetic moment is located in the interstitial region, i.e., away from the atomic nuclei. As a reminder, in the FLAPW method the space is divided into nonoverlapping muffin-tin spheres, which are centered around each atom, and the remaining interstitial region. The muffin-tin radii of N and C, relevant in this case, are chosen to be about 1 Å each.

The second family of compounds are the binary VAs, CrAs, and MnAs. The interest in them started to grow in 2000 when Akinaga and his collaborators managed to grow a multilayers CrAs/GaAs structure.[68] CrAs was found to adopt the zinc-blende structure of GaAs. It was predicted to be a half-metal, and the experimentally determined total spin magnetic moment was found to be in agreement with this prediction.[68] Several studies followed this initial discovery, and electronic structure calculations have confirmed that also similar binary XY compounds, where X is an early transition-metal atom and Y an sp element, should be half-metals.[69,70] The energy gap is located in the minority-spin electronic band structure and is created from the p-d hybridization effect. The TM d orbitals of t_{2g} symmetry transform according to the same symmetry operations as the p valence states of the sp atom, which enables hybridization among them. In the majority-spin bands, the bonding hybrids are mainly of d character, while

in the minority-spin band structure the bonding hybrids are of p character leading (if we also take into account the single deep-lying s valence states) to a $Z_t - 8$ Slater-Pauling rule for the total spin magnetic moment.

The last family of HM magnets under study are the Heusler compounds. These systems have been widely studied because the half metallicity in the bulk samples is well established,[6] and most of them have very high Curie temperatures approaching or even exceeding 1000 K.[71] The first compound that was predicted to be a half-metal was NiMnSb,[4] but most of the research attention during the last years has been focused on the full-Heusler compounds. This family of materials encompasses many more members with diverse magnetic properties. There are strong ferromagnets like Co_2MnSi and Co_2FeAl, ferrimagnets like Mn_2VAl and Mn_2VSi, and even HM antiferromagnets like Cr_2FeGe and Cr_2CoGa. Especially, HM antiferromagnets, initially predicted by van Leuken and de Groot,[72] are of interest as they combine half-metallicity with a zero total net magnetization, which is ideal for spintronics devices due to the vanishing external stray fields created by them; we should add that thin films of Cr_2CoGa have been grown experimentally,[73] a material that has been predicted to exhibit extremely high Curie temperature.[74] The hybridization that gives rise to the bands responsible for the formation of the energy gap is complicated and has been extensively discussed in the literature together with the resulting Slater-Pauling rules (see Ref. [75] for half-Heusler compounds, Ref. [76] for the usual $L2_1$-type Heusler compounds, and Ref. [77] for the inverse XA-type Heuslers). All compounds under study are half-metals, and the atom-resolved spin magnetic moments are in good agreement with previously published data. Here, we should also note that Co_2FeSi, should have a total spin magnetic moment of 6 μ_B in case of half-metallicity. Standard GGA calculations yield a spin magnetic moment of about 5.5 μ_B, and the Fermi level is below the energy gap. Calculations within the LDA$+U$ method[14] or the GW approximation[78] restore the HM character shifting the Fermi level in the gap. On the other hand, recent results by Meinert and collaborators show that a self-consistent calculation fixing the total spin magnetic moment to 6 μ_B reproduces more accurately the position of the band with respect to available experimental data.[79]

B. Effective on-site Coulomb interaction parameters

1. Binary compounds

We start with the discussion of the results of Coulomb interaction parameters for the sp-electron ferromagnets (see Table II). In these compounds, no d valence states are present. The p states of N (C) form bands that are disentangled from the rest of the band structure with some small admixture of Ca (Sr, Ba) s states. Hence these bands lend themselves for the construction of MLWFs forming the correlated subspace. In the case of two nitrides, CaN and SrN, the existence of an energy gap above the Fermi energy (see Ref. [61]) leads to a less efficient screening of the p electrons and, as a consequence, we obtain larger Coulomb matrix elements (see Table II). The calculated intraorbital U exceeds 4 eV for the nitrides, which is comparable to the values for the elementary TMs presented in Ref. [35], while for the carbides the calculated values are

TABLE II. Calculated average partially screened (U_{LDA+U}, U, U', and J) and fully screened ($\tilde{U}$, $\tilde{U}'$, and $\tilde{J}$) Coulomb interaction parameters between the localized orbitals denoted in the second row (in eV) for all HM magnets. We note that unscreened (bare) Coulomb matrix elements (results not shown) for $3d$ atoms in HM magnets are similar to the ones in elementary $3d$ TMs presented in Ref. [35].

Compound	Orbital	U_{LDA+U}	U	U'	J	$\tilde{U}$	$\tilde{U}'$	$\tilde{J}$
CaN	N-$2p$	3.90	4.56	3.57	0.52	0.67	0.16	0.27
SrN	N-$2p$	3.70	4.33	3.38	0.51	0.60	0.13	0.25
SrC	C-$2p$	3.04	3.52	2.80	0.40	1.01	0.44	0.30
BaC	C-$2p$	2.67	3.10	2.45	0.37	0.75	0.29	0.26
VAs	V-$3d$	1.98	2.80	1.77	0.53	1.21	0.43	0.40
CrAs	Cr-$3d$	1.67	2.57	1.45	0.57	1.61	0.64	0.48
MnAs	Mn-$3d$	1.73	2.63	1.50	0.56	1.87	0.84	0.51
FeMnSb	Fe-$3d$	2.16	3.10	1.92	0.60	0.88	0.20	0.36
	Mn-$3d$	3.06	4.02	2.82	0.59	1.56	0.61	0.46
CoMnSb	Co-$3d$	2.31	3.33	2.05	0.64	1.34	0.43	0.46
	Mn-$3d$	2.80	3.72	2.57	0.58	1.63	0.68	0.47
NiMnSb	Ni-$3d$	2.70	3.83	2.42	0.70	2.24	1.04	0.60
	Mn-$3d$	2.65	3.55	2.42	0.56	2.00	0.99	0.50
Mn_2VAl	Mn-$3d$	2.89	3.84	2.65	0.60	1.13	0.33	0.39
	V-$3d$	3.06	3.95	2.84	0.55	1.51	0.61	0.43
Mn_2VSi	Mn-$3d$	3.09	4.10	2.84	0.63	1.19	0.34	0.41
	V-$3d$	3.32	4.25	3.09	0.58	1.62	0.67	0.45
Cr_2FeGe	Cr^A-$3d$	3.05	3.98	2.82	0.58	1.18	0.36	0.40
	Cr^B-$3d$	3.21	4.21	2.96	0.63	1.03	0.25	0.41
	Fe-$3d$	3.46	4.56	3.19	0.69	1.16	0.30	0.42
Cr_2CoGa	Cr^A-$3d$	3.26	4.20	3.02	0.59	1.33	0.45	0.43
	Cr^B-$3d$	3.23	4.22	2.98	0.63	1.21	0.36	0.42
	Co-$3d$	3.84	5.02	3.55	0.73	1.41	0.43	0.48
Co_2CrAl	Co-$3d$	3.74	4.89	3.45	0.72	1.61	0.56	0.50
	Cr-$3d$	2.82	3.68	2.60	0.54	0.85	0.21	0.32
Co_2CrSi	Co-$3d$	3.80	4.95	3.51	0.71	1.88	0.76	0.53
	Cr-$3d$	2.73	3.55	2.53	0.51	1.04	0.33	0.35
Co_2MnAl	Co-$3d$	3.40	4.53	3.12	0.70	1.64	0.60	0.50
	Mn-$3d$	3.23	4.17	3.00	0.58	1.58	0.64	0.45
Co_2MnSi	Co-$3d$	3.28	4.40	3.00	0.70	1.83	0.74	0.53
	Mn-$3d$	3.07	3.98	2.84	0.57	1.71	0.75	0.46
Co_2FeAl	Co-$3d$	3.00	4.06	2.73	0.66	1.68	0.66	0.49
	Fe-$3d$	3.43	4.49	3.17	0.66	1.99	0.89	0.53
Co_2FeSi	Co-$3d$	3.07	4.11	2.81	0.65	1.70	0.68	0.49
	Fe-$3d$	3.40	4.43	3.14	0.64	1.33	0.43	0.46

about 1 eV smaller. The interorbital Coulomb matrix element U' follows the same trend: it is about 3.5 eV for the nitrides and below 3 eV for the carbides. The behavior of U and U' is reflected also in U_{DFT+U} (Hubbard U), which is close to 4 eV for the nitrides and 1 eV less for the carbides. We should note here that as we move from Ca to Sr or from Sr to Ba, although the number of valence electrons does not change, the increase of the lattice constant leads to a narrowing of the p bands, which gives rise to a more efficient screening of the Coulomb interaction and consequently to smaller matrix elements.[81] The value of the Hund exchange parameter J is considerably smaller than the Coulomb repulsion terms. Its value is around 0.4–0.5 eV for these compounds. As we discussed above, we exclude the $p \rightarrow p$ transitions in the polarization function when calculating the partially screened Coulomb interaction. If we include these transitions, we get

the fully screened Coulomb matrix elements $\tilde{U}$, $\tilde{U}'$, and $\tilde{J}$, which are much smaller than the corresponding U, U', and J as expected.[35]

In the case of the binary ferromagnets that contain a TM element (VAs, CrAs, and MnAs), the situation is more complicated. Now, the correlated subspace is composed of the valence d states of the TM atoms. Due to the tetrahedral symmetry, the d states are split into the triply degenerate t_{2g} and doubly degenerate e_g states. The former transform in the same way as the valence p states of As. So, they can hybridize and they do so strongly. Therefore we construct the five Wannier d orbitals out of eight electronic bands, five d and three p bands. We thus have a case of entangled bands for which we employ the procedure outlined in Sec. II. The U values in VAs, CrAs, and MnAs amount to about 2.6–2.8 eV. These values are small when compared with the values for the elementary TMs in Ref. 35, where we found them to be about 3 eV for V and around 4 eV for Cr and Mn. The difference can be attributed to the very efficient screening produced by the As p electrons. Thus, we expect the correlation to be weak in these compounds and to have only a small influence on the electronic structure. The Hund exchange parameter J is slightly above 0.5 eV, while it is around 0.6–0.7 eV in elementary TMs. Interestingly, taking into account in addition the screening inside the correlated subspace, i.e., considering $\tilde{U}$, $\tilde{U}'$, $\tilde{J}$ values, does not reduce the values as drastically as we have observed in the *sp*-electron ferromagnets. Finally, we would like to note that the Hubbard U parameter for CrAs was already calculated in Ref. 24 by employing the cLDA method. The authors obtained a value of 7 eV, which is much larger than our value of 1.67 eV (see Table II). As mentioned in the introduction, this unreasonably large value obtained within cLDA can be attributed to the difficulties in compensating for the self-screening error of the localized electrons (see Ref. 33 for a detailed discussion).

2. Heusler compounds

Finally, we will discuss the case of Heusler compounds, which are the most widely studied HM magnets. Now, there are two different kinds of 3d TM atoms in the unit cell, and the calculation of the Coulomb matrix elements becomes more heavy. In the construction of the Wannier functions for the TM atoms, we include 13 bands for the semi-Heusler compounds and 18 bands for the full-Heusler compounds, taking into account not only the 3d states of the TM atoms but also the valence p states of the nonmagnetic *sp* atom. In half-metallic Heusler compounds, the width of the d bands is usually around 6 eV as can be deduced from several published plots of the density of states (DOS).[75,76] This large value of the band width is due to the strong hybridization of the d and p valence states of the neighboring atoms. It is larger than the calculated U values presented later in this section, and thus half-metallic Heuslers should be classified as weakly correlated materials. We do not present the band structures here since for most HMs, and Heusler compounds in particular, several publications have already been dedicated to describe their band structures in detail.[2,3,75,76]

In the series of the semi-Heusler compounds XMnSb with X = Fe, Co, Ni, where in each substitution the valence d
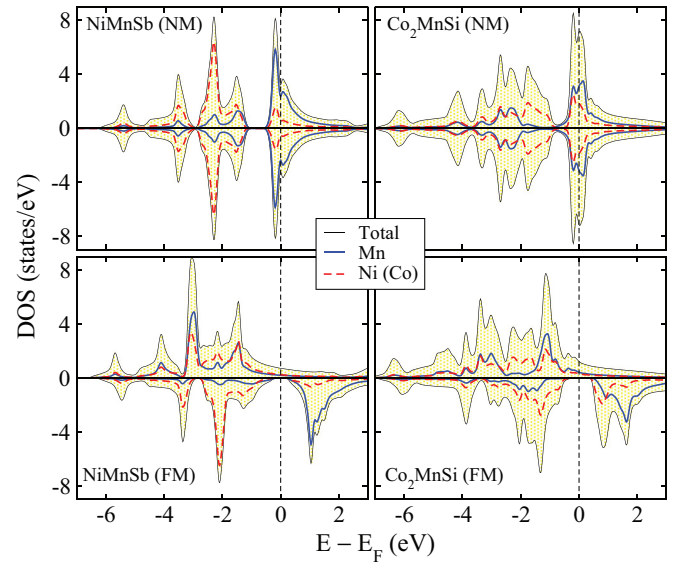

FIG. 2. (Color online) Total and atom-resolved density of states (DOS) for nonmagnetic and magnetic NiMnSb and Co_2MnSi. The zero of the energy axis corresponds to the Fermi level. Positive (negative) DOS values are associated with the majority (minority) spin electrons.

electrons increase by one, we observe a decrease of the U value for the Mn d orbitals from 4.02 to 3.55 eV, while simultaneously the U value for d orbitals at the X atom increases from about 3.1 eV for Fe to 3.83 eV for Ni (see Table II). The increase of U for the X atom can be qualitatively understood on the basis of the behavior of the Mn and X 3d states (see Fig. 2 for the atom resolved DOS of NiMnSb and Refs. 82 and 83 for CoMnSb and FeMnSb). The Fe atom is close to half-filling. In the DOS of FeMnSb there is thus a strong Fe 3d weight around the Fermi level (see Ref. 83) giving rise to efficient screening of the Coulomb interaction through $d \rightarrow sp$ transitions; the closer the occupied and unoccupied states are to the Fermi level, the larger the polarization (see next section for a detailed discussion). As the 3d-electron number of the X atom increases, the 3d weight around the Fermi level decreases and, as a consequence, the Coulomb interaction parameters increase. A similar trend is observed in the matrix elements of the fully screened Coulomb interaction ($\tilde{U}$, $\tilde{U}'$, and $\tilde{J}$), which can be explained by the same arguments. In the case of the elementary 3d TM series, the U value shows a plateau around 4 eV from Cr to Ni, while the presently calculated values for the X atom are considerably smaller. This indicates that the crystal field and the hybridization between the orbitals of the neighboring atoms have a crucial impact on the U values, considerably altering the screening of the orbitals in question. The same conclusion stands also for the interorbital U' parameter, while the Hund exchange parameter J is much less affected by the crystal field or the chemical formula of the compounds.

In the case of the two HM ferrimagnets (Mn_2VAl and Mn_2VSi), the U values for the Mn atoms approach that of elementary Mn. For the nonmagnetic elementary bcc V the U value is about 3 eV, while in the two compounds under study it exceeds 4 eV. This difference can be easily explained

by the spin polarization of the V $3d$ states in these Heusler compounds. As will be discussed in the following section and as it has been shown in Ref. 46 for the case of Fe, Co, and Ni, the spin polarization has a strong influence on the screening of the Coulomb interaction giving rise to larger U values due to the decreased weight of the $3d$ states around the Fermi level. The same discussion holds also for these two Heusler compounds. The Hund exchange J in elementary bcc V is about 0.6 eV, almost identical to its value in the present two Heusler compounds. The small difference as we move from Al to Si for all calculated parameters is due to the smaller lattice constant of the Mn$_2$VSi compound, which leads to a slightly larger Coulomb repulsion between the $3d$ electrons.

The rest of the compounds are full Heusler alloys, where the first two are antiferromagnetic and in the XA structure, while the others are ferromagnetic and exhibit a L2$_1$ structure. Here, the calculated U parameters show a more complex behavior. The Cr atoms exhibit a large variation of U between the XA-type and the L2$_1$-type compounds, which are about 4.0–4.2 eV in the former and about 3.5–3.7 eV in the latter. Also, J is reduced from 0.6 eV in the XA-type compounds to 0.5 in the L2$_1$-type compounds. There are two inequivalent Cr atoms per unit cell in the XA-type compounds with different chemical environments. Each has eight nearest neighbors of which four are Cr atoms and the other four are Fe (Co) atoms in the one case and Ge (Ga) atoms in the other. In the L2$_1$-type compounds Co$_2$CrAl and Co$_2$CrSi, each Cr atom has eight Co atoms as nearest neighbors. The different hybridization with the neighboring atoms influences the values of the calculated parameters. The Mn atoms in Co$_2$MnAl and Co$_2$MnSi show U values close to those of the Mn atoms in the ferrimagnetic compounds discussed in the previous paragraph. The $3d$ orbitals of Fe have a U value of about 4.4–4.5 eV and a J value of 0.65–0.70 eV nearly irrespective of the chemical type of the compounds. The larger deviations are observed for the Co atoms. The U values range from 4.1 eV in Co$_2$FeSi up to 5.0 eV in Cr$_2$CoGa, while J changes about 0.1 eV for Co $3d$ orbitals between the various compounds. The fully screened Coulomb interaction parameters do not show as much variation. They are substantially reduced with respect to the partially screened values.

So far, we have only focused on the on-site Coulomb interaction parameters. Due to metallic screening in TM-based HM magnets, the calculated nearest-neighbor U values turn out to be negligibly small, i.e, they lie between 0.1 and 0.4 eV as in the $3d$ TM series.[35] On the other hand, the situation is different for sp-electron ferromagnets for which we obtain sizable nearest-neighbor U values (0.5–0.7 eV) for p orbitals. This is because the p bands, which form the Fermi surface, are isolated in these systems; thus partial screening is not metallic.

Similar to the case of CrAs, previous cLDA calculations of the effective Coulomb interaction for the $3d$ TMs in NiMnsb and Co$_2$MnSi resulted in Hubbard U values of about 6 eV,[11,18] which are found to be too large to be used in material-specific LDA + DMFT calculations. Thus, in LDA + DMFT studies addressing the correlation effect in ferromagnetic NiMnSb and Co$_2$MnSi, the Hubbard U and Hund exchange J for the $3d$ TMs are chosen to be 3 and 0.9 eV,[11,18] respectively, which is very close to our calculated values (see Table II).

C. Orbital dependence of U and $\bar{U}$

As we have already mentioned above, the values presented in Table II for the TM atoms are the average ones of the Coulomb matrix elements. The lattice structures presented in Fig. 1 exhibit tetrahedral symmetry, and the valence $3d$ states thus separate into the doubly degenerate e_g and the triply degenerate t_{2g} states. Within the tetrahedral symmetry group, the former are lower in energy, while in the octahedral symmetry group, it is vice versa. This is well understood in terms of the relative orientations of the orbitals in space. For the structures under study, the e_g orbitals point along the coordinate axes. Figure 1 shows that in this direction atoms of the same kind are relatively far away with a different atom in between. The nearest neighbors of the same element are in the direction of the t_{2g} orbitals. As a result, the intraorbital Coulomb matrix elements show a variation with the orbital character. In Table III, we present the calculated U and $\tilde{U}$ values for the e_g and t_{2g} orbitals of the TM atoms in NiMnSb and Co$_2$MnSi. The energetic position of the e_g and t_{2g} states are reflected in the calculated Coulomb matrix elements. The screening for the former is less effective, and we thus get larger Coulomb matrix elements. We note in passing that the corresponding bare interaction parameters are very similar, which rules out that a different spread of the Wannier functions is responsible for the variation. The difference in the calculated U values between the two different subsets of the d orbitals is about 0.5 eV for Ni and Co and 0.2–0.3 eV for Mn. These values are slightly larger than for the elementary TMs in Ref. 35 where, e.g., for Ni the difference is only 0.14 eV. However, the difference is still comparatively small so that we can safely say that the average values presented in Table II will capture the essential characteristics of the correlations in these compounds. We also note that if we take into account the full screening, the obtained $\tilde{U}$ values for the e_g and t_{2g} orbitals in the heavier Ni and Co atoms are almost identical, while for Mn a larger difference persist.

In Table III, we have also included in parentheses the values for the case of non-spin-polarized calculations, which differ substantially from the spin-polarized case, especially the fully screened Coulomb interaction. A similar behavior has been observed in the elementary TMs[46] and can be explained with the help of the DOS for the magnetic and nonmagnetic systems presented in Fig. 2. First, we remark that in the nonmagnetic calculations the Fermi level is located in a peak of the DOS. Due to the Stoner criterion, both NiMnSb and Co$_2$MnSi therefore prefer the ferromagnetic ground state. The variations

TABLE III. Partially screened U and fully screened $\tilde{U}$ for e_g and t_{2g} orbitals (in eV) for the ferromagnetic NiMnSb and Co$_2$MnSi compounds. We also show the results for the nonmagnetic state in parentheses.

	NiMnSb		Co$_2$MnSi	
	Ni	Mn	Co	Mn
$U(e_g)$	4.08 (4.66)	3.65 (2.83)	4.69 (4.47)	4.17 (3.86)
$U(t_{2g})$	3.66 (4.22)	3.48 (2.72)	4.22 (4.10)	3.85 (3.62)
$\tilde{U}(e_g)$	2.40 (2.25)	2.10 (0.60)	1.87 (0.69)	1.96 (0.34)
$\tilde{U}(t_{2g})$	2.14 (1.81)	1.92 (0.54)	1.81 (1.23)	1.54 (0.76)

in Coulomb matrix elements between the ferromagnetic and the nonmagnetic state (see Table III) can be qualitatively explained by the DOS around the Fermi level. As the screened Coulomb interaction U depends on the polarizability [see Eq. (3)], the number of occupied and unoccupied states around the Fermi level plays an important role in determining its strength. Mn in nonmagnetic NiMnSb has the largest DOS around the Fermi energy and hence the smallest Coulomb matrix elements with an average U value of about 2.7–2.8 eV. Ni in nonmagnetic NiMnSb, on the contrary, has the smallest DOS around the Fermi level among the TM atoms in the two compounds and thus the largest calculated U values. In the nonmagnetic state of Co_2MnSi, we observe a density of Co and Mn derived states at the Fermi level that is in-between that of the Ni and Mn atoms in NiMnSb (the one of Mn being slightly larger than that of Co), which is reflected by the calculated U values. For the ferromagnetic compounds, on the other hand, the corresponding peaks are shifted to lower and higher energies for the majority and minority spin, respectively, due to the exchange field, leading to a lower DOS around the Fermi level. As a consequence, we obtain larger Coulomb matrix elements in the ferromagnetic state compared to the nonmagnetic state for all TM atoms in NiMnSb and Co_2MnSi.

D. Frequency dependence of U and J

The Coulomb interaction parameters presented in Table II are for the static limit, i.e., for $\omega = 0$. The question arises whether the use of the static limit of the Coulomb interaction in model Hamiltonians is justified. In Fig. 3, we present the frequency dependence $U(\omega)$ and $J(\omega)$ for selected HM magnets: CaN, CrAs, NiMnSb, and Co_2MnSi. In the case of the two Heusler compounds, the $U(\omega)$ is almost constant at low frequencies up to 15 eV, suggesting that the use of the static value $U(\omega = 0)$ in model Hamiltonians is appropriate. As we approach the plasma frequency, slightly above 15 eV, $U(\omega)$ increases rapidly approaching the unscreened (bare) value, i.e., at high frequencies screening is not effective anymore.
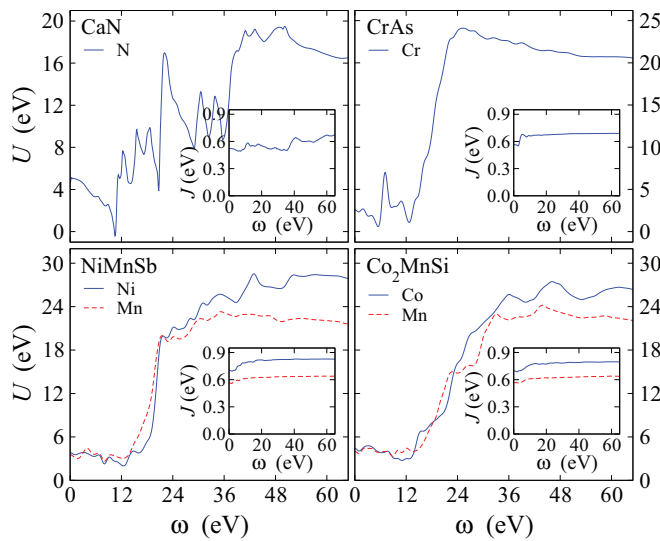

FIG. 3. (Color online) Frequency dependence of the effective Coulomb interaction parameters $U(\omega)$ and $J(\omega)$ for the HM ferromagnetic CaN, CrAs, NiMnSb, and Co_2MnSi compounds.

TABLE IV. Effect of the p electrons on the screening of the Coulomb interaction parameters for CrAs, NiMnSb, and Co_2MnSi. In parentheses we show the results from Table II for comparison. The notation $pd \to pd$ means that $d \to d$ and $d \to p$ transitions are excluded in the calculation of the polarization function.

Comp.	Orb.	$U(pd \to pd)$	$U'(pd \to pd)$	$J(pd \to pd)$
CrAs	Cr-3d	5.67 (2.57)	4.42 (1.45)	0.63 (0.57)
NiMnSb	Ni-3d	5.43 (3.83)	3.95 (2.42)	0.74 (0.70)
	Mn-3d	5.22 (3.55)	4.04 (2.42)	0.59 (0.56)
Co_2MnSi	Co-3d	5.76 (4.40)	4.32 (3.00)	0.72 (0.70)
	Mn-3d	5.29 (3.98)	4.12 (2.84)	0.58 (0.57)

For the binary compounds, the situation is very different. The frequency-dependent $U(\omega)$ of the Cr 3d electrons shows strong variations at low frequencies, while for the 2p electrons of N in CaN the static approximation fails completely as we have very strong oscillations of $U(\omega)$ even at low frequencies. In contrast to $U(\omega)$, the Hund exchange parameter $J(\omega)$, being mostly an atomic property, depends only weakly on the frequency and does not show significant variations at the plasma frequency. Especially in the case of the d electrons, it is almost constant in the plotted frequency range. This atomiclike behavior of $J(\omega)$ can be attributed to the fact that the exchange charge has no $l = 0$ component, which makes $J(\omega)$ almost immune to screening, except at very low frequencies.

E. Role of the sp atom in the screening

Finally, we discuss the effect played by the nonmagnetic sp atom in the screening of the Coulomb interaction between the TM 3d electrons in CrAs, NiMnSb, and Co_2MnSi. To study this effect, we have excluded also the $d \to p$ transitions in the calculation of the polarization function in addition to the $d \to d$ transitions. The obtained values for the Coulomb matrix elements are presented in Table IV. For comparison, we have also included the U, U', and J in parentheses from Table II. When additionally excluding the $d \to p$ transitions, the U values become similar for all compounds under study and amount to about 5.5 eV. The $d \to p$ screening channel is quite efficient in the case of CrAs, where the U increases more than a factor of two with respect to its value of Table II, from 2.57 eV to 5.67 eV, while J remains relatively unaffected. In the case of Ni and Mn in NiMnSb, the U values become larger by about 30% when including the additional screening channel. In Co_2MnSi, the difference in U values calculated with and without the $d \to p$ screening channel is very small. As we move from CrAs to NiMnSb and then to Co_2MnSi, the number of 3d electrons as well as of s electrons in the unit cell increases and, as a consequence, the screening of the p electrons of the nonmagnetic sp atom is not so efficient any more. Note that the Coulomb screening is not additive. An extended discussion of this issue can also be found in Ref. 33.

IV. CONCLUSIONS

We have calculated the strength of the effective on-site Coulomb interaction (Hubbard U and Hund exchange J) between localized electrons in different classes of HM magnets employing the cRPA method within the FLAPW framework.

We have considered (i) *sp*-electron ferromagnets in rock-salt structure, (ii) zinc-blende 3*d* binary ferromagnets, and (iii) ferromagnetic and ferrimagnetic semi- and full-Heusler compounds. For HM *sp*-electron ferromagnets, the calculated Hubbard *U* parameters are between 2.7 and 3.9 eV, while for TM-based HM compounds they lie between 1.7 and 3.8 eV, being smallest for MnAs (Mn 3*d* orbitals) and largest for Cr$_2$CoGa (Co 3*d* orbitals). We have found that for the HM full-Heusler compounds the obtained Hubbard *U* values are comparable to those in elementary 3*d* TMs, while for the semi-Heusler compounds the Hubbard *U* values are slightly smaller. We have shown that the increase of the Hubbard *U* parameter with structural complexity, i.e., from MnAs to Cr$_2$CoGa, can be attributed to an efficient screening of the *p* electrons of the nonmagnetic *sp* atoms. The *p* electron screening turns out to be more efficient for MnAs than for Cr$_2$CoGa. Our calculated Hubbard *U* parameters for CrAs, NiMnSb, and Co$_2$MnSi are about two times smaller than previous estimates based on the cLDA method. Furthermore,

the band width of the studied compounds are in most cases smaller than the calculated Hubbard *U* parameters. The HM magnets can thus be classified as weakly correlated materials.

The Coulomb interaction parameters play an important role in the construction of model Hamiltonians aimed to the study of correlation effects in the electronic structure of HM magnets. Strong correlations give rise to nonquasiparticle states above (or below) the Fermi energy at finite temperatures reducing the spin polarization and, as a consequence, the efficiency of spintronics devices. We hope that the Hubbard *U* and Hund exchange *J* values presented here will prove helpful for future LDA+*U* and LDA + DMFT calculations as well as for other methods applied to describe correlation effects in HM magnets.

*e.sasioglu@fz-juelich.de

†galanakis@upatras.gr

[1] I. Žutić, J. Fabian, and S. Das Sarma, Rev. Mod. Phys. **76**, 323 (2004).

[2] M. I. Katsnelson, V. Yu. Irkhin, L. Chioncel, A. I. Lichtenstein, and R. A. de Groot, Rev. Mod. Phys. **80**, 315 (2008).

[3] K. Sato, L. Bergqvist, J. Kudrnovský, P. H. Dederichs, O. Eriksson, I. Turek, B. Sanyal, G. Bouzerar, H. Katayama-Yoshida, V. A. Dinh, T. Fukushima, H. Kizaki, and R. Zeller, Rev. Mod. Phys. **82**, 1633 (2010).

[4] R. A. de Groot, F. M. Mueller, P. G. van Engen, and K. H. J. Buschow, Phys. Rev. Lett. **50**, 2024 (1983).

[5] W. E. Pickett and H. Eschrig, J. Phys.: Condens. Matter **19**, 315203 (2007).

[6] C. Felser, G. H. Fecher, and B. Balke, Angew. Chem. Int. Ed. **46**, 668 (2007).

[7] S. Chadov, T. Graf, K. Chadova, X. Dai, F. Casper, G. H. Fecher, and C. Felser, Phys. Rev. Lett. **107**, 047202 (2011).

[8] M. Ležaić, Ph. Mavropoulos, J. Enkovaara, G. Bihlmayer, and S. Blügel, Phys. Rev. Lett. **97**, 026404 (2006).

[9] Ph. Mavropoulos, M. Ležaić, and S. Blügel, Phys. Rev. B **72**, 174428 (2005).

[10] S. Sugahara and J. Nitta, Proc. IEEE **98**, 2124 (2010).

[11] L. Chioncel, Y. Sakuraba, E. Arrigoni, M. I. Katsnelson, M. Oogane, Y. Ando, T. Miyazaki, and E. Burzo, and A. I. Lichtenstein, Phys. Rev. Lett. **100**, 086402 (2008).

[12] K. Karlsson, F. Aryasetiawan, and O. Jepsen, Phys. Rev. B **81**, 245113 (2010).

[13] I. V. Solovyev, J. Phys.: Condens. Matter **20**, 293201 (2008).

[14] H. C. Kandpal, G. H. Fecher, C. Felser, and G. Schönhense, Phys. Rev. B **73**, 094422 (2006).

[15] A. Yamasaki, L. Chioncel, A. I. Lichtenstein, and O. K. Andersen, Phys. Rev. B **74**, 024419 (2006).

[16] J. Minár, J. Phys.: Condens. Matter **23**, 253201 (2011).

[17] F. Lechermann, A. Georges, A. Poteryaev, S. Biermann, M. Posternak, A. Yamasaki, and O. K. Andersen, Phys. Rev. B **74**, 125120 (2006).

[18] L. Chioncel, M. I. Katsnelson, R. A. de Groot, and A. I. Lichtenstein, Phys. Rev. B **68**, 144425 (2003).

[19] S. Chadov, J. Minár, H. Ebert, A. Perlov, L. Chioncel, M. I. Katsnelson, and A. I. Lichtenstein, Phys. Rev. B **74**, 140411(R) (2006).

[20] H. Allmaier, L. Chioncel, E. Arrigoni, M. I. Katsnelson, and A. I. Lichtenstein, Phys. Rev. B **81**, 054422 (2010).

[21] L. Chioncel, E. Arrigoni, M. I. Katsnelson, and A. I. Lichtenstein, Phys. Rev. Lett. **96**, 137203 (2006).

[22] L. Chioncel, E. Arrigoni, and M. I. Katsnelson, and A. I. Lichtenstein, Phys. Rev. B **79**, 125123 (2009).

[23] L. Chioncel, Ph. Mavropoulos, M. Ležaić, S. Blügel, E. Arrigoni, M. I. Katsnelson, and A. I. Lichtenstein, Phys. Rev. Lett. **96**, 197203 (2006).

[24] L. Chioncel, M. I. Katsnelson, G. A. de Wijs, R. A. de Groot, and A. I. Lichtenstein, Phys. Rev. B **71**, 085111 (2005).

[25] L. Chioncel, I. Leonov, H. Allmaier, F. Beiuşeanu, E. Arrigoni, T. Jurcuţ, and W. Pötz, Phys. Rev. B **83**, 035307 (2011).

[26] T. Kotani, J. Phys.: Condens. Matter **12**, 2413 (2000).

[27] I. V. Solovyev and M. Imada, Phys. Rev. B **71**, 045103 (2005).

[28] I. Schnell, G. Czycholl, and R. C. Albers, Phys. Rev. B **65**, 075103 (2002).

[29] P. H. Dederichs, S. Blügel, R. Zeller, and H. Akai, Phys. Rev. Lett. **53**, 2512 (1984).

[30] V. I. Anisimov and O. Gunnarsson, Phys. Rev. B **43**, 7570 (1991); M. Cococcioni and S. de Gironcoli, *ibid*. **71**, 035105 (2005).

[31] K. Nakamura, R. Arita, Y. Yoshimoto, and S. Tsuneyuki, Phys. Rev. B **74**, 235113 (2006).

[32] F. Aryasetiawan, M. Imada, A. Georges, G. Kotliar, S. Biermann, and A. I. Lichtenstein, Phys. Rev. B **70**, 195104 (2004).

[33] F. Aryasetiawan, K. Karlsson, O. Jepsen, and U. Schönberger, Phys. Rev. B **74**, 125106 (2006).

[34] T. Miyake and F. Aryasetiawan, Phys. Rev. B **77**, 085122 (2008); T. Miyake, F. Aryasetiawan, and M. Imada, *ibid*. **80**, 155134 (2009).

[35] E. Şaşıoğlu, C. Friedrich, and S. Blügel, Phys. Rev. B **83**, 121101(R) (2011).

[36] T. O. Wehling, E. Şaşıoğlu, C. Friedrich, A. I. Lichtenstein, M. I. Katsnelson, and S. Blügel, Phys. Rev. Lett. **106**, 236805 (2011).

[37] B.-C. Shih, Y. Zhang, W. Zhang, and P. Zhang, Phys. Rev. B **85**, 045132 (2012); B.-C. Shih, T. A. Abtew, X. Yuan, W. Zhang, and P. Zhang, *ibid*. **86**, 165124 (2012); R. Sakuma and F. Aryasetiawan, *ibid*. **87**, 165118 (2013).

[38] H. Sims, W. H. Butler, M. Richter, K. Koepernik, E. Şaşıoğlu, C. Friedrich, and S. Blügel, Phys. Rev. B **86**, 174422 (2012).

[39] Y. Nomura, M. Kaltak, K. Nakamura, C. Taranto, S. Sakai, A. Toschi, R. Arita, K. Held, G. Kresse, and M. Imada, Phys. Rev. B **86**, 085117 (2012); Y. Nomura, K. Nakamura, and R. Arita, *ibid*. **85**, 155452 (2012).

[40] http://www.flapw.de

[41] J. P. Perdew, K. Burke, and M. Ernzerhof, Phys. Rev. Lett. **77**, 3865 (1996).

[42] N. Marzari and D. Vanderbilt, Phys. Rev. B **56**, 12847 (1997).

[43] A. A. Mostofi, J. R. Yates, Y.-S. Lee, I. Souza, D. Vanderbilt, and N. Marzari, Comput. Phys. Commun. **178**, 685 (2008).

[44] F. Freimuth, Y. Mokrousov, D. Wortmann, S. Heinze, and S. Blügel, Phys. Rev. B **78**, 035120 (2008).

[45] C. Friedrich, S. Blügel, and A. Schindlmayr, Phys. Rev. B **81**, 125102 (2010).

[46] E. Şaşıoğlu, A. Schindlmayr, C. Friedrich, F. Freimuth, and S. Blügel, Phys. Rev. B **81**, 054434 (2010).

[47] L. Vaugier, H. Jiang, and S. Biermann, Phys. Rev. B **86**, 165105 (2012).

[48] J. Hubbard, Proc. R. Soc. London A **276**, 238 (1963); J. Kanamori, Prog. Theor. Phys. **30**, 275 (1963); M. C. Gutzwiller, Phys. Rev. Lett. **10**, 159 (1963).

[49] V. I. Anisimov, I. V. Solovyev, M. A. Korotin, M. T. Czyzyk, and G. A. Sawatzky, Phys. Rev. B **48**, 16929 (1993).

[50] S. L. Dudarev, G. A. Botton, S. Y. Savrasov, C. J. Humphreys, and A. P. Sutton, Phys. Rev. B **57**, 1505 (1998).

[51] P. Baettig, C. Ederer, and N. A. Spaldin, Phys. Rev. B **72**, 214105 (2005).

[52] V. I. Anisimov, F. Aryasetiawan, and A. I. Lichtenstein, J. Phys.: Condens. Matter **9**, 767 (1997).

[53] E. R. Ylvisaker, W. E. Pickett, and K. Koepernik, Phys. Rev. B **79**, 035103 (2009).

[54] S. Y. Savrasov, A. Toropova, M. I. Katsnelson, A. I. Lichtenstein, V. Antropov, and G. Kotliar, Z. Kristallogr. **220**, 473 (2005).

[55] F. Bultmark, F. Cricchio, O. Grånäs, and L. Nordström, Phys. Rev. B **80**, 035121 (2009).

[56] E. Bousquet and N. Spaldin, Phys. Rev. B **82**, 220402(R) (2010).

[57] K. Kusakabe, M. Geshi, H. Tsukamoto, and N. Suzuki, J. Phys.: Condens. Matter **16**, S5639 (2004).

[58] A. Laref, E. Şaşıoğlu, and I. Galanakis, J. Phys.: Condens. Matter **23**, 296001 (2011).

[59] G. Y. Gao, K. L. Yao, and N. Li, J. Phys.: Condens. Matter **23**, 075501 (2011).

[60] M. Sieberer, J. Redinger, S. Khmelevskyi, and P. Mohn, Phys. Rev. B **73**, 024404 (2006).

[61] M. Geshi, K. Kusakabe, H. Nagara, and N. Suzuki, Phys. Rev. B **76**, 054433 (2007).

[62] K. Özdoğan, E. Şaşıoğlu, and I. Galanakis, J. Appl. Phys. **111**, 113918 (2012).

[63] G. Y. Gao and K. L. Yao, Appl. Phys. Lett. **91**, 082512 (2007).

[64] G. Y. Gao, K. L. Yao, E. Şaşıoğlu, L. M. Sandratskii, Z. L. Liu, and J. L. Jiang, Phys. Rev. B **75**, 174442 (2007).

[65] S. Dong and H. Zhao, Appl. Phys. Lett. **98**, 182501 (2011).

[66] J. C. Slater, Phys. Rev. **49**, 931 (1936).

[67] L. Pauling, Phys. Rev. **54**, 899 (1938).

[68] H. Akinaga, T. Manago, and M. Shirai, Jpn. J. Appl. Phys. **39**, L1118 (2000).

[69] I. Galanakis and P. Mavropoulos, Phys. Rev. B **67**, 104417 (2003).

[70] Ph. Mavropoulos and I. Galanakis, J. Phys.: Condens. Matter **19**, 315221 (2007).

[71] P. J. Webster and K. R. A. Ziebeck, in *Alloys and Compounds of d-Elements with Main Group Elements. Part 2*, edited by H. R. J. Wijn, Landolt-Börnstein, New Series, Group III, Vol. 19, Pt.c (Springer-Verlag, Berlin 1988), pp. 75–184.

[72] H. van Leuken and R. A. de Groot, Phys. Rev. Lett. **74**, 1171 (1995).

[73] T. Graf, F. Casper, J. Winterlik, B. Balke, G. H. Fecher, and C. Felser, Z. Anorg. Allg. Chem. **635**, 976 (2009).

[74] I. Galanakis and E. Şaşıoğlu, Appl. Phys. Lett. **99**, 052509 (2011).

[75] I. Galanakis, P. H. Dederichs, and N. Papanikolaou, Phys. Rev. B **66**, 134428 (2002).

[76] I. Galanakis, P. H. Dederichs, and N. Papanikolaou, Phys. Rev. B **66**, 174429 (2002).

[77] S. Skaftouros, K. Özdoğan, E. Şaşıoğlu, and I. Galanakis, Phys. Rev. B **87**, 024420 (2013).

[78] M. Meinert, C. Friedrich, G. Reiss, and S. Blügel, Phys. Rev. B **86**, 245115 (2012).

[79] M. Meinert, J.-M. Schmalhorst, M. Glas, G. Reiss, E. Arenholz, T. Böhnert, and K. Nielsch, Phys. Rev. B **86**, 054420 (2012); M. Meinert, *ibid*. **87**, 045103 (2013).

[80] E. Şaşıoğlu, I. Galanakis, L. M. Sandratskii, and P. Bruno, J. Phys.: Condens. Matter **17**, 3915 (2005).

[81] E. Şaşıoğlu, C. Friedrich, and S. Blügel, Phys. Rev. Lett. **109**, 146401 (2012).

[82] H. M. Huang, S. J. Luo, and K. L. Yao, Physica B **406**, 1368 (2011).

[83] R. A. De Groot, A. M. van der Kraan, and K. H. J. Buschow, J. Magn. Magn. Mater. **61**, 330 (1986).